ADVANCING EARTH AND SPACE SCIENCES

JGR Atmospheres

RESEARCH ARTICLE
10.1029/2025JD045713

Dry Versus Humid Heat Seasonality and Drivers in the North American Monsoon Region

Catherine C. Ivanovich[1,2], Benjamin I. Cook[1,3], and Sonali McDermid[1,4]

[1]NASA Goddard Institute for Space Studies, New York, NY, USA, [2]NASA Postdoctoral Program Fellow, Oak Ridge Associated Universities, NASA NPP Program, Oak Ridge, TN, USA, [3]Division of Ocean Climate Physics, Lamont-Doherty Earth Observatory, Palisades, NY, USA, [4]Department of Environmental Studies, New York University, New York, NY, USA

Key Points:

- In the North American Monsoon region, dry and humid heat are distinct in overall seasonality and the timing of individual extreme events
- Drivers of dry heat extremes are spatially and temporally consistent, associated with moisture reductions and atmospheric ridges
- The relative importance of temperature versus humidity in driving humid heat extremes depends on monsoon propagation and variability

Supporting Information:

Supporting Information may be found in the online version of this article.

Correspondence to:

C. C. Ivanovich,
cci2107@columbia.edu

Citation:

Ivanovich, C. C., Cook, B. I., & McDermid, S. (2026). Dry versus humid heat seasonality and drivers in the North American monsoon region. *Journal of Geophysical Research: Atmospheres*, *131*, e2025JD045713. https://doi.org/10.1029/2025JD045713

Received 24 OCT 2025
Accepted 20 MAY 2026

Author Contributions:

Conceptualization: Catherine C. Ivanovich, Benjamin I. Cook, Sonali McDermid
Data curation: Catherine C. Ivanovich
Formal analysis: Catherine C. Ivanovich
Funding acquisition: Catherine C. Ivanovich, Benjamin I. Cook, Sonali McDermid
Methodology: Catherine C. Ivanovich, Benjamin I. Cook, Sonali McDermid
Project administration: Benjamin I. Cook, Sonali McDermid
Software: Catherine C. Ivanovich
Supervision: Benjamin I. Cook, Sonali McDermid
Validation: Catherine C. Ivanovich

Abstract The Southwest United States and northwestern Mexico are well-known for their extreme dry heat, but these regions also experience humid heat extremes when the North American Monsoon (NAM) is active. Here, we investigate the distinct seasonality, dynamics, and drivers of dry versus humid heat in the NAM region. We find that the dry heat season can peak up to 38 days earlier than the humid heat season, with only 40%–60% overlap in the seasons on average in the core of the monsoon. Atmospheric ridges and reduced surface moisture are key drivers of extreme dry heat, consistent across space and time. In contrast, the regional dynamics of extreme humid heat are seasonally dependent. During the peak of the monsoon season, when ample moisture is available, extreme humid heat is driven by elevated dry bulb temperatures that occur alongside suppressed precipitation. However, during the shoulder months of the monsoon with lower background moisture availability, humid heat extremes are associated with elevated precipitation, soil moisture, and specific humidity. Our results identify the NAM region as possessing distinct dry and humid heat seasonalities and where the climatic drivers of humid heat depend on their timing relative to the monsoon season.

Plain Language Summary The Southwest United States and northwestern Mexico are two regions which experience both dry and humid heat extremes. In this article, we explore how these two types of extreme heat differ in their seasonality and identify their individual drivers. We find that the dry and humid heat seasons are relatively distinct. The dry heat season peaks significantly earlier than the humid heat season, and only about half of the days during the two heat seasons overlap in the wettest parts of the monsoon region. During June through September, extreme dry heat throughout the study region occurs in the presence of reduced surface moisture and atmospheric ridges. In contrast, the relative dependence of extreme humid heat on temperature versus humidity changes with the evolution of seasonal monsoon precipitation and background moisture availability.

1. Introduction

The Southwest United States and northwestern Mexico are well-established hotspots for extreme heat. As arid subtropical deserts, these regions receive a large amount of incoming solar radiation during the warm season, and their dry land surfaces partition a high fraction of the surface energy balance into sensible heat. These dynamics fuel extreme temperatures, which are frequent, intense, and long-lasting, three heat wave characteristics that are increasing with climate change (Cueto et al., 2010; Mutiibwa et al., 2015; Perkins-Kirkpatrick & Lewis, 2020). However, one often overlooked aspect of extreme heat in this region is the seasonality of the events themselves (Dong et al., 2024; Rogers et al., 2021). Extreme heat events taking place outside of a region's traditional heat season can place exaggerated strain on human health, as individuals may be unprepared to implement heat management strategies or lack acclimatization (De Freitas & Grigorieva, 2015). The extreme heat season in Phoenix in 2024 is a poignant example, with a reported unprecedented 113 consecutive days above 100°F during the summer. This was followed by a secondary period of 21 record-breaking temperature days in October (Chow, 2024; Freedman, 2024), an additional persistent heat event occurring after the typical extreme heat season. Investigating how the drivers of extreme heat events vary seasonally is therefore critical for constraining their predictability and improving our understanding of how seasonal risks may be shifting with climate change.

Another underappreciated characteristic of extreme heat in the Southwest United States and northwestern Mexico, and one strongly connected to moisture seasonality in these regions, is the occurrence of high absolute values of both dry and humid heat (Rogers et al., 2021). Dry bulb temperatures typically peak in the pre-monsoon

Visualization: Catherine C. Ivanovich
Writing – original draft: Catherine C. Ivanovich
Writing – review & editing: Catherine C. Ivanovich, Benjamin I. Cook, Sonali McDermid

season, as the precipitation associated with monsoon onset increases shading and evaporative cooling at the surface (Lizárraga-Celaya et al., 2010). However, on the edge of the monsoon system, high temperatures can be sustained even during the wet season (Sheppard et al., 2002). The influence on humid heat from monsoon systems and precipitation is generally more complicated due to the simultaneous influence of temperature, wind speed and direction, solar insolation, and humidity (e.g., Ambika et al., 2024; C. C. Ivanovich, Horton, et al., 2024). The joint impact of these variables on intensifying humid heat can be maximized through a variety of combinations, for example, during light intermittent rain, which can moisten soils to enhance surface evaporation without dramatically decreasing solar radiation, amplifying humid heat (Zhang et al., 2024). Further, the relative influence of these controls can fluctuate throughout the year on various timescales based on the background mean climate and intraseasonal variability (C. Ivanovich et al., 2022; Raymond et al., 2017).

Distinguishing between extreme dry and humid heat is essential for preparing for their individual impacts. While dry heat has larger effects on plant health (Abatzoglou & Williams, 2016; Bowman et al., 2009; Schauberger et al., 2017; Ting et al., 2023), with implications for agricultural production and ecosystem stability, humid heat is expected to have higher impacts on human health due to its influence over the efficiency through which humans cool down via sweating (Buzan & Huber, 2020; Fanger, 1970; Mora et al., 2017; Parsons, 2006; Sherwood & Huber, 2010; Steadman, 1979). Because mitigation and adaptation strategies for dry versus humid heat are distinct (Matthews et al., 2025), identifying when each heat type occurs is essential for targeted exposure reduction and emergency management planning. However, while dry heat extremes in the Southwest United States and northwestern Mexico have been extensively discussed (e.g., Cueto et al., 2010; Guirguis et al., 2018; McKinnon et al., 2021; Navarro-Estupiñan et al., 2018), little work has been done investigating humid heat dynamics and their seasonality in these same regions (Johnson et al., 2024; Raymond et al., 2017). Research has shown that the degree to which the timing of extreme dry and humid heat intersects varies across the globe (Raymond et al., 2020; Rogers et al., 2021), including in regions affected by the North American Monsoon (Johnson et al., 2024; Raymond et al., 2017; Rogers et al., 2021). In other arid regions, extreme humid heat days often occur in relatively close proximity to precipitation events (Speizer et al., 2022). Raymond et al. (2017) further identified that the temperature versus humidity contributions toward extreme humid heat events can differ throughout the warm season in the Southwest US. Nevertheless, the complex interactions between the North American Monsoon and local heat seasons in the Southwest United States and northwestern Mexico have been underexplored, motivating an explicit investigation.

In this analysis, we characterize the seasonal and daily scale drivers of dry versus humid heat in the North American monsoon region. We focus on this region because of its frequent exceedance of high absolute dry and humid heat thresholds and the complex influences of regional monsoon dynamics on temperature, humidity, solar insolation, and wind speed—variables known to modulate humans' experience of heat stress. To capture variation in all four of these variables, we investigate dry and humid heat extremes defined using 2-m air temperature (T_a) and wet bulb globe temperature (WBGT), respectively. To facilitate our analysis, we devise a concise, novel method to define local heat seasons which can be applied broadly around the globe. Finally, we composite a range of meteorological variables on extreme Ta and WBGT events to explore how conditions evolve in space and time during extreme events. Through these analyses, we aim to answer the following questions about the study region:

1. How distinct is the timing of dry and humid heat in terms of seasonality and individual extreme events?
2. What background climate characteristics facilitate extreme dry versus humid heat events?
3. What daily scale physical mechanisms generate dry and humid heat extremes?
4. How different are these relationships across space, that is, on the edge of the North American Monsoon system compared to within its core?

2. Methods

2.1. Data

We use gridded reanalysis data for the historical period from 1980 to 2024 because of its continuity and high temporal and spatial resolution, which enables exploration of both local mechanisms triggering single-day extreme events and large-scale dynamics which shape overall seasonal patterns. Hourly data were retrieved from the Modern-Era Retrospective analysis for Research and Applications, Version 2 (MERRA-2), including 2-m temperature (T_a), 2-m dew point temperature, surface pressure, water surface layer 1, surface latent heat flux, surface sensible heat flux, and precipitation. These hourly values were used to calculate daily mean, daily maximum, and daily total values, where applicable. MERRA2 and other reanalysis products have been used widely throughout published literature to explore dry and humid heat extreme dynamics (e.g., Bekris et al., 2023; Engdaw et al., 2022; Raymond et al., 2024) and have been evaluated against observational data sets (e.g., Rogers et al., 2021). Using reanalysis data is also necessitated by our calculation of daily maximum wet bulb globe temperature, which requires inputs of variables (temperature, humidity, radiation, and wind data) often unavailable from hourly observational station data.

Hourly wet bulb globe temperatures (WBGT) were calculated using the *thermofeel* toolbox (Brimicombe et al., 2022). This toolbox calculates WBGT using globe temperature as in De Dear, 1987, calculated via mean radiant temperature as defined by Di Napoli et al., 2020. These methods have been validated against the Liljegren method (Brimicombe et al., 2022; Liljegren et al., 2008) and used throughout the literature for analyses of extreme humid heat (e.g., Khan et al., 2025; Parajuli et al., 2025). In addition to 2-m temperature and 2-m dew point temperature, other required fields included 10-m eastward wind, 10-m northward wind, surface incoming shortwave flux, surface net downward shortwave flux, surface absorbed longwave radiation, and surface net downward longwave flux. From the hourly WBGT calculations, we then aggregated to the daily maximum WBGT and used this metric for our extreme humid heat analyses.

Reanalysis products including MERRA2 have demonstrated surface moisture biases (Hirschi et al., 2025), which may be particularly relevant to the present study due to our investigation of the complex interactions of heat and monsoon dynamics. To evaluate the sensitivity of our results to potential moisture biases in the underlying data, results of all primary analyses are repeated using equivalent variables from the fifth major global reanalysis of the European Center for Medium-Range Weather Forecasts (ERA5; Hersbach et al., 2020) and are provided in Supporting Information S1 (Figures S1–S6). These two reanalyses have opposing global mean surface moisture biases relative to remote sensing products, with literature showing that MERRA2 and ERA5 tend to have wet and dry biases, respectively (Hirschi et al., 2025). However, the magnitude of these biases is minimized over the North American Monsoon region studied here. Additionally, we find that the overall interpretation of our results does not change between these two data sets, indicating that the results presented here are robust against a range of surface moisture biases. Any minor differences in identified patterns are described in the Results section. We also note that both of these reanalysis products do not explicitly represent urban areas, which can exhibit fine scale variations in the component variables used to calculate WBGT (Shonk et al., 2026). The impact of this limitation is minimized by exploration of regional rather than highly localized patterns in dry and humid heat.

2.2. Methods

2.2.1. Humid Heat Metric Choice

While there exists a variety of humid heat metrics in the climate science literature, no one-size-fits-all metric best captures the influence of meteorology on humans' experience of heat stress (Grundstein & Vanos, 2021). We select WBGT for this study because it is currently one of the most widespread humid heat metrics used in the United States to monitor heat stress in areas ranging from occupational heat stress standards for outdoor workers to high school athletics (Binkley et al., 2002; OSHA Technical Manual, 2017). WBGT has been shown to better reflect humans' physiological response to heat stress conditions compared to other metrics such as wet bulb temperature and Heat Index (Buzan et al., 2015; Vecellio et al., 2022a, Vecellio et al., 2022b) and includes the contributions of temperature, humidity, solar insolation, and wind speed toward humid heat, all variables that can be modulated by the monsoon. When measured in outdoor environments, WBGT can be expressed as

$$\mathrm{WBGT} = 0.7T_w + 0.2T_g + 0.1T_a \tag{1}$$

where T_w is the natural wet bulb temperature (incorporating measurements of air temperature and humidity), T_g is the globe thermometer temperature (incorporating measurements of air temperature, solar insolation, and wind speed), and T_a is the dry bulb temperature.

A characteristic of all joint humid heat metrics is that, by definition, high thresholds of humid heat can be generated by a variety of combinations of temperature and humidity (C. C. Ivanovich, Sobel, et al., 2024). Not all combinations place the same physiological strain on human health, and high thresholds of humid heat created by hot-dry environments have been shown to be more dangerous than those created by warm-humid environments

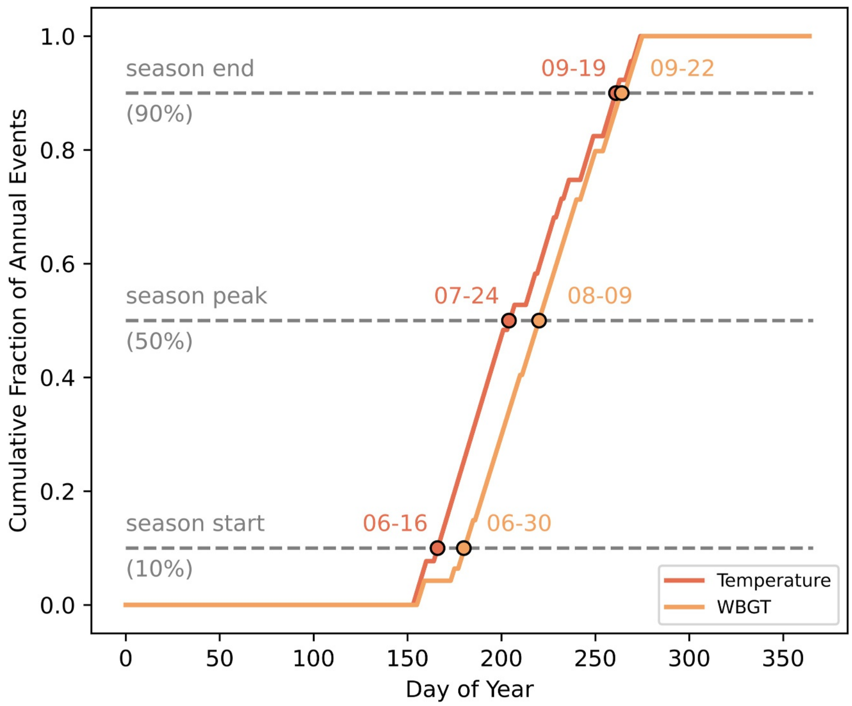

Figure 1. Example dry and humid heat season calculation for one grid cell in Phoenix, AZ during the year 2010. Analysis uses dry heat defined by Tmax and humid heat defined by WBGTmax, calculated from hourly MERRA2 data.

(Budd, 2008; Vanos & Grundstein, 2020; Vecellio et al., 2022a, Vecellio et al., 2022b). To address this challenge in identifying dangerous thresholds of extreme humid heat, we use regionally specific extreme heat warning thresholds as defined by the National Weather Service to reflect the climatology of temperature and humidity in the study region (Grundstein et al., 2015).

2.2.2. Heat Season Definition

We devise a novel method for defining the onset, peak, and demise of a heat season in a given location. The method follows the derivation in Cook & Buckley, 2009 to determine the onset and withdrawal of the monsoon season in Southeast Asia. At each grid cell, we select the historical time series for the daily maximum temperature (T_{max}). We then select the "high heat days" which surpass the 75th percentile of Tmax across the full historical record. This identifies an average of roughly 91 heat days per year across the historical record, but the exact number of heat days will vary year-to-year. We define the start of the annual heat season as the day when 10% of the cumulative annual events have occurred, and the end of the heat season as the day when 90% of these events have occurred. Heat season duration is defined as the number of days between the start and end of the heat season, reflecting the spread of high heat days throughout the calendar year. We also calculate the peak in the heat season as the median of this cumulative distribution. We repeat this process for the humid heat season using daily maximum WBGT (WBGTmax). Figure 1 visualizes the result of these calculations for one grid cell in Phoenix, AZ during the year 2010. The interannual variability in these calculations for this grid cell is shown in Figure S7 in Supporting Information S1. We perform a series of sensitivity tests using 20% and 80% cumulative thresholds for the start and end dates of the season, as well as using the 85th percentile of the selected daily maximum heat variable across the historical record to identify high heat days. While the individual dates identified using these thresholds are different, the overall qualitative patterns in terms of which heat type peaks first, which type of heat season is longer, and spatial variations in these measures, for example, are all consistent across these ranges of tests (not shown).

2.2.3. Extreme Event Composites

In addition to the seasonality of dry and humid heat, we explore the conditions associated with both extreme types. We first characterize the background climates which lead to high or low frequencies of extreme events to identify

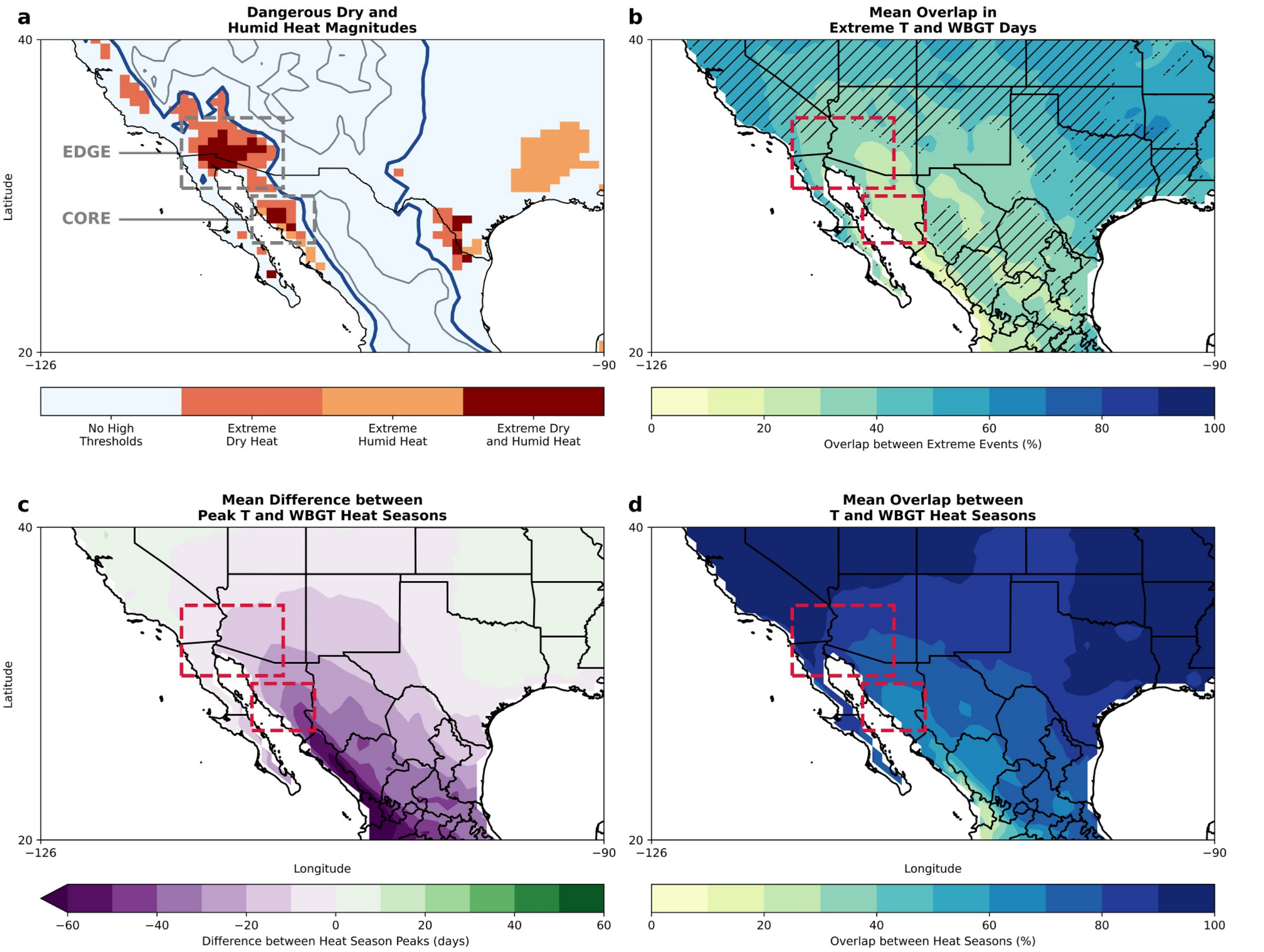

Figure 2. Study region identification based on dry vs. humid heat magnitudes and timing. (a) Locations experiencing T95 over 40°C and WBGT95 over 30.05°C. Regional boxes of interest labeled as "EDGE" and "CORE." Elevation in contours at intervals of 750 m, starting at 1,000 m above sea level in thick blue contour. (b) Shading indicates the percent overlap in T95 and WBGT95 events. Hatching indicates grid cells which experience the highest climatological frequency of T95 and WBGT95 days during the same month. (c) Historical mean difference in T_a and WBGT heat season peak. (d) Historical mean percent overlap in T_a and WBGT heat seasons.

the baseline conditions which shape the overall timing and seasonality of extreme heat events. We identify 95th percentile daily maximum temperature and WBGT days (T95 and WBGT95) based on the full calendar year and across the full historical record (1980–2024). We then calculate the monthly total number of 95th percentile days within each region which occur during June–September (JJAS) throughout the historical period, as these are the only months during which both regions have experienced both extreme types. We identify the upper and lower tercile of these months in the historical record with respect to T95 and WBGT95 frequency and analyze the anomalous monthly climatologies of these high versus low frequency extreme event months. We also explore the evolution of daily scale meteorology the week before and after T95 and WBGT95 events in each region during JJAS to identify shorter term drivers of these extreme events.

3. Results

3.1. Identifying Dry and Humid Heat Seasons

Both dry and humid heat can reach dangerous magnitudes in the Southwest US and northwestern Mexico (Figure 2a). We identify grid cells whose 95th percentile T_a (T95) and 95th percentile WBGT (WBGT95) magnitudes surpass thresholds shown to impact human health, 40°C T_a and 30.05°C WBGT, respectively. The T_a threshold defines exposure to "extreme heat strain," even with short duration exposure and accompanied by moderate humidity levels (Asseng et al., 2021). The WBGT threshold is based on the U.S. National Weather Service's "General Threshold for WBGT," as the entry point into the "high risk for heat related illness" in Category 3 regions, locations which often experience high thresholds for extreme humid heat and where residents may be better acclimated to extreme temperatures (Grundstein et al., 2015). Two regions which surpass these dangerous thresholds are in the edge and core of the North American Monsoon region (e.g., Adams & Comrie, 1997, Figure S9 in Supporting Information S1), henceforth referred to as "EDGE" and "CORE." The EDGE region includes all grid cells which exceed both thresholds in box 117–110.5°W and 30.5–35°N, including the populous cities of Phoenix, AZ and Mexicali, MX. The CORE region is to the east of the Gulf of California, including points which surpass the required thresholds in the box spanning 112.5–108.5°W and 27–30°N and includes cities such as Hermosillo, MX. Monthly climatology for each region are plotted in Figure S10 in Supporting Information S1. In these regions, magnitudes of T95 are up to 45.2°C and WBGT95 magnitudes reach 31.4°C. These regions are at low elevation and topographically bounded, as shown by the blue 1 km elevation contour in Figure 2a. They also border the Gulf of California, the primary moisture source for the North American Monsoon (Boos & Pascale, 2021; Mitchell et al., 2002). There is a third region exceeds dangerous dry and humid heat thresholds at the border of southern Texas and northeastern Mexico. Because weather in this region is driven more strongly by flow from the Gulf of Mexico than the North American Monsoon (Kimmel et al., 2016), influencing both the local drivers and seasonality of precipitation, we do not explore this region further in the present analysis.

We find that the timing of T_a and WBGT extremes and seasons is more distinct in the EDGE and CORE regions than in much of North America. Only about 20%–40% of individual T95 events are also recorded as WBGT95 events in EDGE and CORE (Figure 2b). Further, the calendar month with the highest frequency of T95 and WBGT95 events is different in both regions (July/August and June/August for EDGE and CORE, respectively; Figure S15 in Supporting Information S1). We devise a novel heat season definition to further explore the spatial and temporal variability of heat seasonality across different metrics. The start, peak, and end of the annual heat season, described in detail in the Methods, is based on the cumulative number of high heat days (dry or humid) that occur each calendar year. The start, peak, and end of the heat season in a given year are defined as the day after which 10, 50, and 90% of high heat days in that year have occurred. Using this definition, we find that the average peak of the T_a heat season can be up to 16 days before the average WBGT heat season peak in the EDGE region, and up to 38 days earlier in the CORE region (Figure 2c; Figure S16 in Supporting Information S1). The T_a heat season also tends to start and end earlier than the WBGT heat season in each region, and the length of the T_a heat season is longer than that of WBGT (Figure S17 in Supporting Information S1). The standard deviation of the start, peak, end, and length of the heat season is larger for T_a than WBGT (Figure S18 in Supporting Information S1). The mean overlap of the two heat seasons as defined by the range of dates between the mean heat season start and end is greater in EDGE than in CORE, with 60%–100% overlap versus 40%–60% overlap, respectively (Figure 2d). Even in the EDGE region where there is higher seasonal overlap than in CORE, it is rare for individual T95 and WBGT95 events to occur on the same day. For comparison, in most of the surrounding United States, the two heat seasons and individual extreme heat events are almost always concurrent.

We proceed by focusing our analysis on the EDGE and CORE regions because they (a) satisfy the criteria for experiencing T95 and WBGT95 at magnitudes relevant to human health, and (b) exhibit distinct timing of dry versus humid heat in terms of individual extreme events and seasonality. Given the separate timing of dry and humid heat in these regions, we wish to evaluate whether their drivers are also distinguishable. To do so, we first characterize the monthly mean background climates that facilitate high versus low frequencies of T95 and WBGT95 extreme events.

3.2. Monthly Scale Background Climates Facilitating Extreme Dry Versus Humid Heat

In both EDGE and CORE, months with relatively high frequencies of T95 events are associated with dry surface background climates (Figure 3; see Figure S19 in Supporting Information S1 for full regional maps without significance masking). In both regions, months with the highest tercile of T95 event counts in months June–September are associated with reduced specific humidity, surface soil moisture, and precipitation relative to months with the lowest tercile of event frequencies. These relative reductions are stronger in magnitude and statistically significant in CORE (significance measured by a Student's *t*-test with p-values below 0.05). The surface and atmosphere in the CORE region are much moister on average during JJAS than in EDGE (Figure S10 in Supporting Information S1). The associated greater cloud cover and higher partitioning of surface energy to the

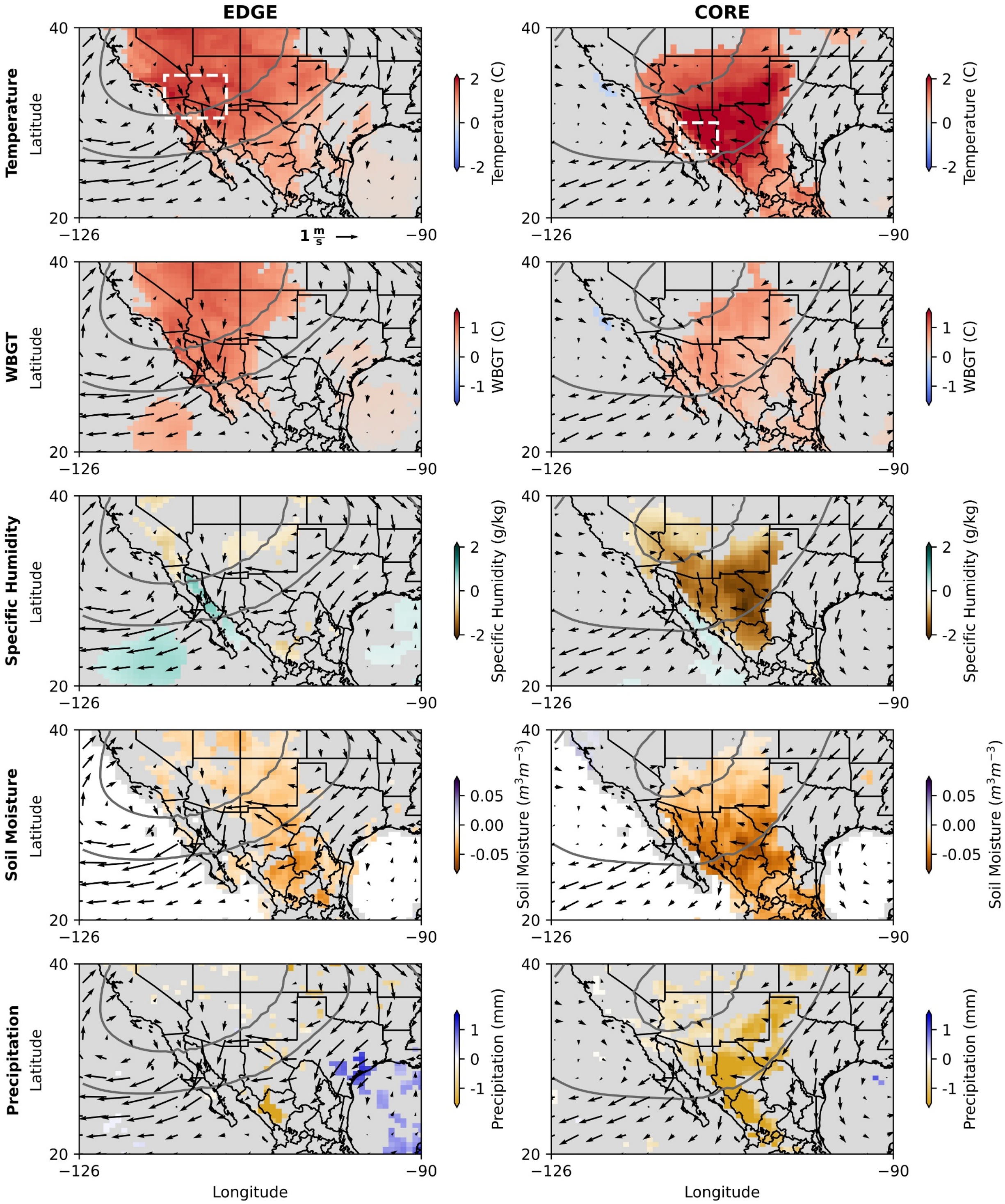

Figure 3. Difference in mean monthly background anomalies during months in JJAS with high versus low frequency of T95 events over EDGE (left) and CORE (right). Light gray shading masks out insignificant shaded patterns. Regional boundaries shown in the top row by white dashed outline. Vectors indicate horizontal winds at 850 hPa. Gray contours show positive geopotential height anomalies at 500 hPa with contour levels from 0 to 30 m with an interval of 10 m. Each column represents the difference in a given variable's anomalies during months in the highest tercile of T95 event frequencies minus the mean anomalies during months in the lowest tercile of T95 event frequencies.

latent versus sensible component resist increases in background T_a, which can be reduced through stronger declines in surface moisture associated with weaker monsoon seasons. During high frequency T95 event months, both regions also experience elevated geopotential heights at 500 hPa (Z500). Large scale wind patterns at 850 hPa are anomalously northerly in both regions, slowing down the climatological influx of relatively cool, moist air from the Gulf of California flowing southeasterly into the EDGE and easterly into the CORE (Figures S11 and S13 in Supporting Information S1). These low-level wind anomalies align closely with the orientation of the atmospheric ridges over each region. Together, these conditions elevate both mean T_a and mean WBGT compared to months with a low frequency of T95 events.

Background climate conditions during months with a high frequency of WBGT95 events are different from those with a high frequency of T95 events, and patterns are less spatially consistent between the two study regions (Figure 4; see Figure S20 in Supporting Information S1 for full regional maps without masking). For both regions, months with high WBGT95 frequency exhibit elevated specific humidity, but with almost three times as large anomalies in EDGE than in CORE (2 g/kg and 0.7 g/kg, respectively) and these anomalies are only statistically significant in CORE. In EDGE, this anomalously high specific humidity is accompanied by positive but insignificant anomalies in both precipitation and soil moisture. At the same time, negative but insignificant T_a anomalies throughout EDGE indicate that the evaporative cooling and shading associated with the elevated precipitation and soil moisture decrease mean T_a. However, the influx of surface moisture is sufficient to offset small decreases in T_a, leading to a net increase in mean WBGT during these months.

In contrast, positive specific humidity anomalies during high frequency WBGT95 months in CORE are accompanied by very weak soil moisture and precipitation anomalies, and all of these differences are statistically insignificant. There is a positive Z500 anomaly over CORE during these months—which is more clearly organized than the Z500 anomalies over EDGE—and stronger positive anomalies in T_a. This heightened mean T_a may facilitate the slightly elevated background specific humidity during these months through the Clausius Clapeyron relationship, as there are a variety of local and advective moisture sources. The North American Monsoon precipitation can increase humidity through evaporation from the land surface and prevailing southerly flow associated with the monsoon circulation can advect moisture from the Gulf of California and Pacific Ocean. Together, these background conditions serve to increase both T_a and specific humidity, intensifying the mean WBGT during these months.

We note that there are slight differences in patterns identified in the background climates when using MERRA2 data (Figures 3 and 4; Figures S19–S20 in Supporting Information S1) versus ERA5 data (Figures S3–S4 and S21–S22 in Supporting Information S1). Namely, during months with a high frequency of T95 events, ERA5 winds at 850 hPa are anomalously northwesterly over EDGE and westerly over CORE. Further, during months with high WBGT95 frequency, both regions experience intensification of T_a and all surface moisture variables, though these anomalies are not statistically significant in ERA5 (Figures S20 and S22 in Supporting Information S1). These differences may be related to the distinct regional surface moisture climatologies in the two data sets (Hirschi et al., 2025), as the mean specific humidity during WBGT95 events is higher in MERRA2 than in ERA5 (Figure S23 in Supporting Information S1). However, our overall interpretation that anomalous background climate moisture plays a stronger role in EDGE while these anomalies are of less importance in CORE is consistent between these two data sources.

We have illustrated that the conducive background conditions can raise mean T_a and WBGT in the CORE and EDGE regions to encourage higher frequencies of extreme dry and humid heat. We next explore how local meteorology drives individual extreme dry and humid heat events once these favorable conditions are in place.

3.3. Daily Scale Meteorological Drivers of Extreme Dry Versus Humid Heat

While the drivers of extreme dry heat are spatially and temporally consistent, the physical mechanisms generating individual humid heat events are seasonally dependent and reflect background moisture availability. In the EDGE region, surface moisture is anomalously low in the week before T95 events, consistent across the heat season (JJAS; Figure 5). Standardized anomalies in specific humidity, precipitation, and soil moisture are also all negative preceding these events. Further, evaporative fraction (EF) is less than the monthly historical mean value in all 4 months of interest and is particularly suppressed during the wettest months of July and August. Incoming shortwave radiation is elevated while wind speeds move from positive to negative anomalies in the week preceding heat extremes during each month. During June and September, T95 events tend to be followed by

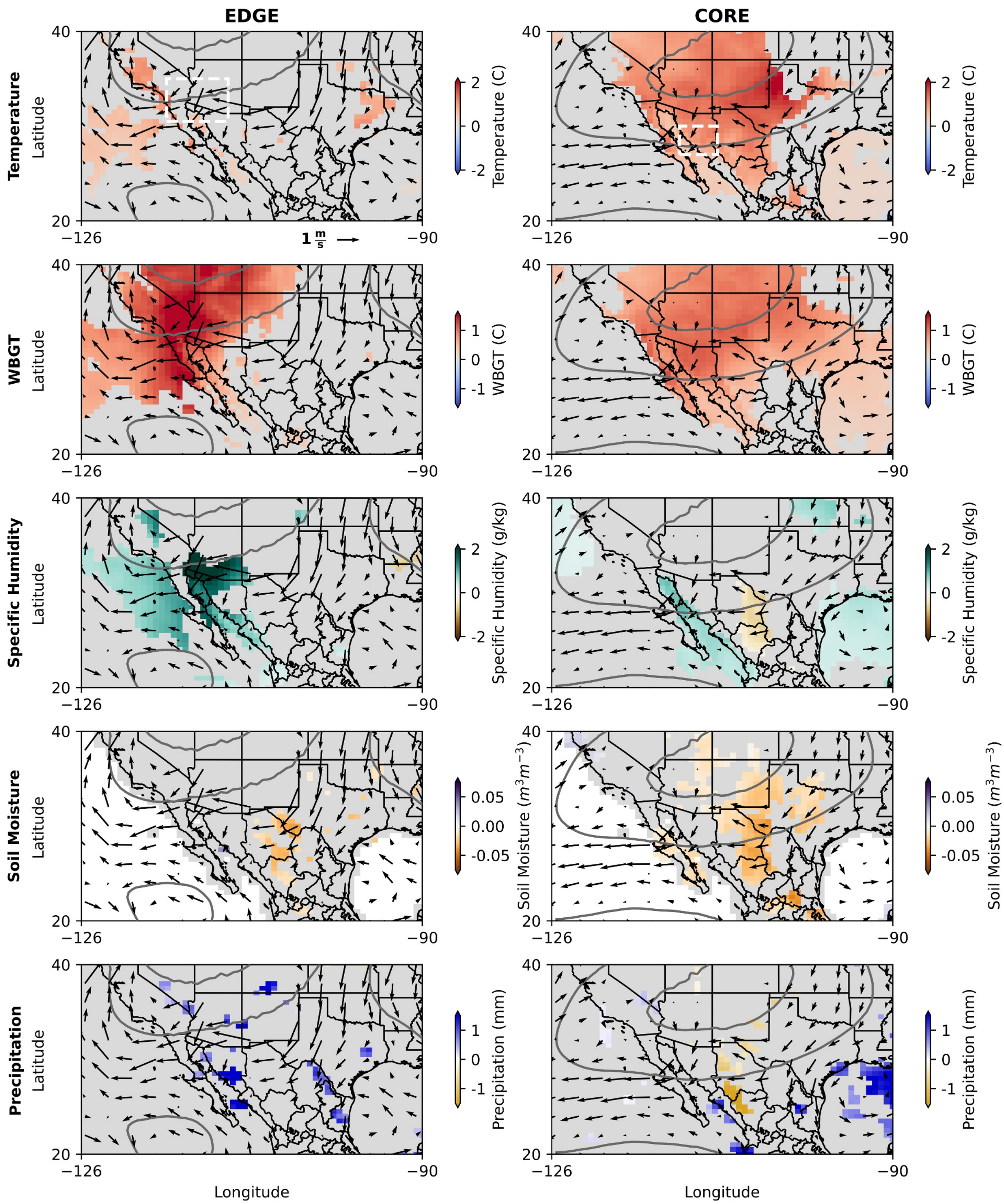

Figure 4. Analogous to Figure 3, but for WBGT95 events.

enhanced precipitation a few days after peak T_a, leading to relative increases in soil moisture, EF, and specific humidity.

The conditions preceding WBGT95 events are significantly different from those before T95 events (Figure S24 in Supporting Information S1, as measured with a Student's t-test with p-values below 0.05), and specific humidity

10.1029/2025JD045713

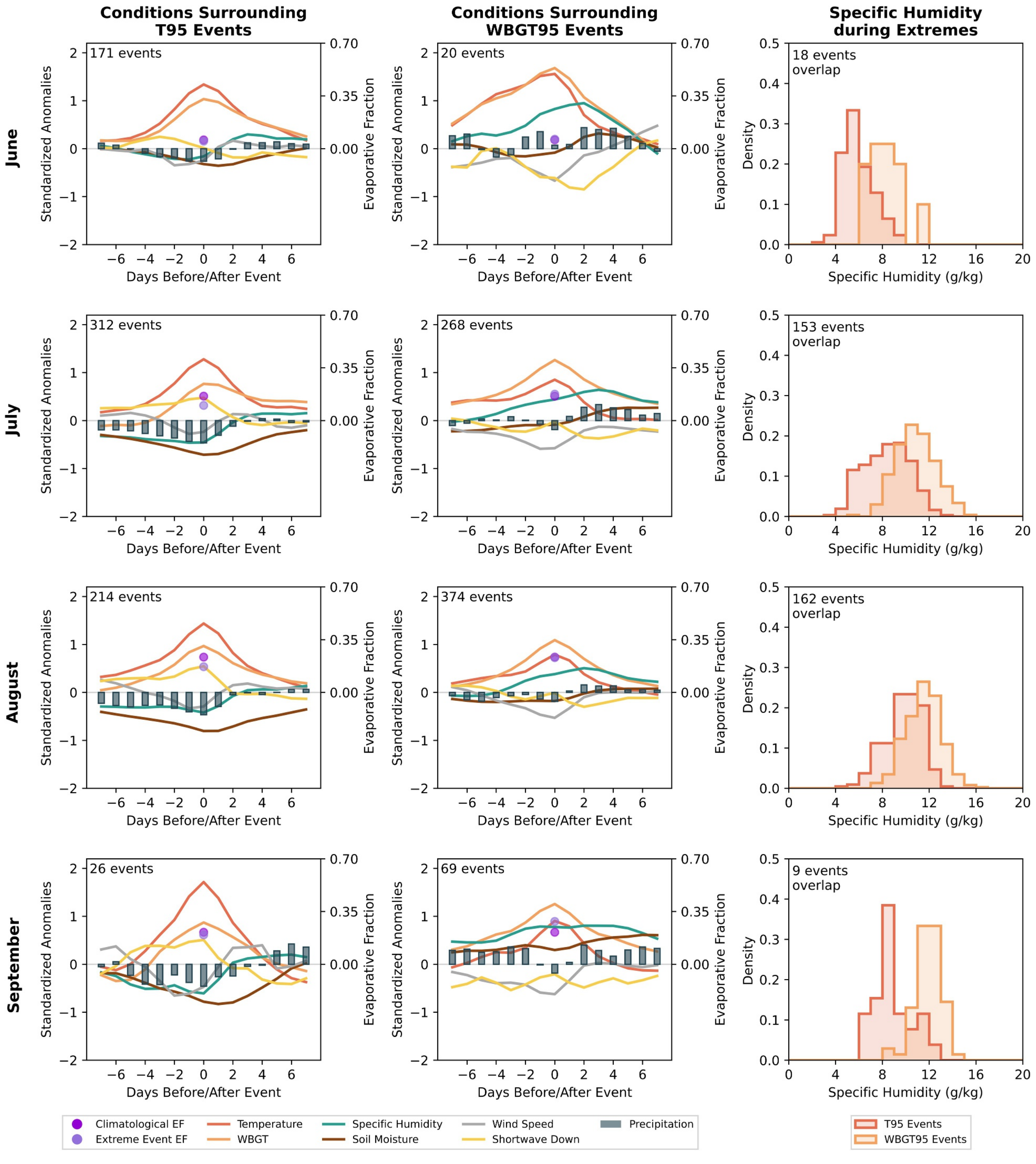

Figure 5. For the EDGE region, evolution of meteorological conditions during the week before and after T95 (left column) and WBGT95 (middle column) events. Right column: Distribution of daily average specific humidity on the day of each extreme event type. Numbers in the upper left corner indicate the number of T95 events (left column), WBGT95 events (middle column), and the overlap between these events (right column) in each month.

tends to be elevated in the days leading up to WBGT95 events in all months in JJAS. During June, when the climatological EF is relatively low, intermittent positive precipitation anomalies precede WBGT95 events. In September, precipitation is strongly enhanced on days −7 to −2 before the WBGT95 event. The anomalies then become neutral on Day −1 and turn negative on Day 0, the day of the WBGT95 event. During the peak months of climatological monsoon precipitation in July and August, precipitation tends to be suppressed during the week before the WBGT95 events. Incoming shortwave radiation evolves alongside these fluctuations in precipitation, predominantly suppressed during June/September and with neutral anomalies during July/August. Temperatures are also elevated during WBGT95 events in June, with smaller positive anomalies in other months. In September, the increases in surface moisture dominate the WBGT anomaly evolution. Because June and September are on the shoulders of the monsoon season when there is a relative lack of precipitation compared to July and August, WBGT95 events require an influx of moisture through another source—whether enhanced local moisture recycling or advection. For example, while 18 of the 20 historical WBGT95 events that happened in the month of June are simultaneously T95 events, there are 171 total June T95 events in the historical record in EDGE. This demonstrates that extreme temperatures alone are insufficient to trigger WBGT95 events in this region and require the addition of anomalous moisture. Indeed, the distributions of specific humidity during T95 and WBGT95 events in the shoulder months are more distinct than during the peak of the monsoon season, indicating that humid heat events are more humidity-driven in June/September and more temperature-driven in July/August. Negative wind speed anomalies during all months intensify in the days leading up to WBGT95 events, increasing heat stress conditions. Across all months, WBGT95 events tend to be followed by enhanced precipitation, with simultaneous increases in soil moisture and EF. Specific humidity anomalies peak a few days after the peak in WBGT and then decline back towards a neutral state with the rapidly decreasing T_a anomalies. This generates an asymmetry in the evolution of WBGT during WBGT95 events, where WBGT anomalies decline more slowly than T_a anomalies due to the additional moisture.

Similar patterns are identified in the CORE region, and seasonal differences in humid heat drivers are even more pronounced than in the EDGE region (Figure 6). CORE experiences suppressed surface moisture in the week preceding T95 events across all months, though with smaller magnitude anomalies in June. This suppressed precipitation is accompanied by elevated incoming shortwave radiation, largest in magnitude during July–September. Wind speed anomalies vary between months but are small on the day of T95 events. Following T95 events, precipitation anomalies are positive during June and September but negligible during July and August. In all months, soil moisture remains suppressed in the week following T95 events, and only in August are slight positive specific humidity anomalies recorded in the days after the event. Conditions preceding WBGT95 events in this region are again significantly different from local dry events (Figure S25 in Supporting Information S1), and those in the shoulder months of the monsoon season tend to be associated with elevated specific humidity even when soil moisture and precipitation anomalies are neutral or negative. During the month of June, the climatological EF in CORE is much lower than during July–September (0.07 vs. 0.4–0.5, respectively), indicating that the region shifts from a moisture-limited toward a more energy-limited evapotranspiration regime. The drivers of WBGT95 events are constrained by the changing availability of moisture at the surface. June WBGT95 events tend to be humidity-driven, building upon high temperatures, as evidenced by the large overlap between T95 and WBGT95 events during this month (24 of 31 WBGT95 events in June are also T95 events). WBGT95 events are more temperature-driven in the peak of the monsoon season, reflected by the increase in EF during the event peak. Increases in solar radiation also fuel WBGT95 events during these months, as anomalies evolve in opposition to those of precipitation. Even in September, when specific humidity is elevated and contributing to the peak in WBGT, soil moisture and precipitation anomalies are negative in the week before the WBGT95 event. The high climatological EF during this month indicates that there is already high background surface moisture in the region, and the positive T_a anomalies can facilitate increases in specific humidity through the Clausius Clapeyron relationship. The neutral wind speed anomalies in July–September acting on top of overall low magnitude wind speeds (Figure S12 in Supporting Information S1) indicate that wind stagnation is playing a smaller role in increasing humid heat than during the month of June. Wind speed anomalies and magnitudes during WBGT95 events are also lower overall in CORE than in EDGE. In all months, WBGT95 events in CORE tend to be followed by enhanced precipitation. Soil moisture and evaporative fraction anomalies both remain negative or neutral in all months except June, with soil moisture recovering as local precipitation increases.

We again note some distinctions between patterns observed in the MERRA2 and ERA5 data sets (Figures 5 and 6 and Figures S5–S6 in Supporting Information S1). Evaporative fraction (both climatological and during extreme events) is lower in MERRA2 than in ERA5 across all months in EDGE and CORE. Windspeed anomalies are closer to neutral in ERA5 than in MERRA2 during WBGT95 events in EDGE, suggesting that wind stagnation drives humid heat extremes to a lesser extent. Additionally, specific humidity recorded during T95 and WBGT95 events are lower in magnitude in both regions in ERA5 than in MERRA2 (Figure S23 in Supporting Information S1). This aligns with the established dry and wet biases for the two data sets, respectively (Hirschi

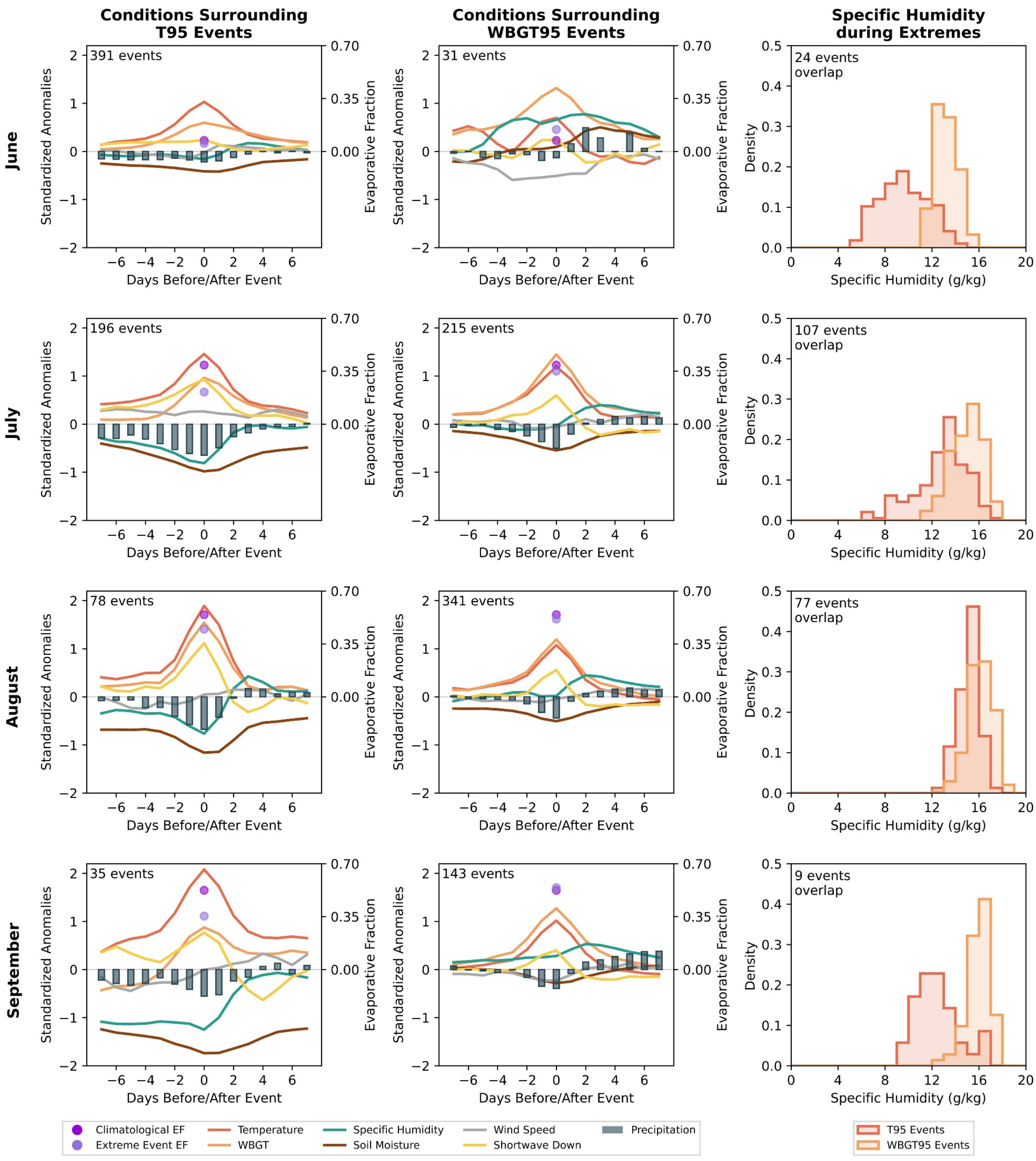

Figure 6. Analogous to Figure 5, but for the CORE region.

et al., 2025). However, standardized specific humidity anomalies play a larger role in generating WBGT95 events during the peak of the monsoon season from July–August in CORE according to ERA5 than MERRA2. Other than these distinctions, the time evolution of standardized anomalies of the surface moisture variables, including specific humidity, soil moisture, and precipitation, are in strong agreement between the two data sets and lead to similar interpretations. Overall, the drivers of extreme dry heat in the North American Monsoon region are consistent across space and time. In contrast, extreme WBGT events can be driven by T_a or specific humidity fluctuations. These controlling mechanisms are seasonally dependent in both study regions, but to a greater extent in CORE.

4. Discussion

We analyze the commonalities and distinctions between the seasonality and drivers of dry and humid heat in two key areas of the North American Monsoon region which experience dangerous thresholds of T_a and WBGT. The EDGE and CORE regions experience relatively distinct dry and humid heat seasonality, with the dry heat season starting, peaking, and ending earlier than that of the humid heat season, as well as being longer in length. The background climates which generate high frequencies of T95 days are similar in EDGE and CORE, featuring positive geopotential height anomalies and surface drying. However, monthly conditions facilitating WBGT95 events differ in these two regions, as EDGE is much more arid than CORE during their respective heat seasons. In EDGE, net increases in mean WBGT are driven by positive anomalies in specific humidity, soil moisture, and precipitation, which compensate for decreases in T_a. In contrast, the humid CORE region experiences a higher frequency of WBGT95 events during months with elevated geopotential height and T_a anomalies. The daily scale meteorology that drives individual extreme events is similar between the two regions. Across all months, T95 events are preceded by further reductions in surface moisture. Extreme WBGT95 events can be temperature- or humidity-driven, depending on the associated background moisture availability. During the shoulder months of the monsoon season when precipitation is ramping up and down, positive specific humidity anomalies play a greater role in WBGT95 events, whether driven by intermittent precipitation intensification (EDGE) or coupled with elevated T_a through the Clausius Clapeyron relationship (CORE).

These results extend previous investigations of extreme humid heat drivers in other monsoon regions by illustrating that the influence of the monsoon on extreme humid heat can vary across both space and time. Recent work has identified spatial variations in the response to the South Asian summer monsoon, demonstrating that relatively arid regions (Pakistan and northwestern India) versus the humid regions (Bangladesh and central and northeastern India) of South Asia experience intensified humid heat during enhanced and suppressed monsoon precipitation, respectively (Ambika et al., 2024; C. C. Ivanovich, Horton, et al., 2024). This is consistent with the background monthly climates identified here that facilitate high frequencies of WBGT95 events in the arid EDGE region and moister CORE region. We further extend this understanding to demonstrate that in the North American Summer Monsoon region, there is not only spatial variation in the drivers of humid heat but also temporal variations in a given location depending on the season.

These results are also consistent with and build upon the literature exploring the drivers of the highest magnitudes of extreme heat experienced globally, in monsoon regions and beyond. Here we find that extreme dry heat is triggered through consistent mechanisms across the region and seasons, which include surface drying and atmospheric ridges—drivers highlighted by many recent analyses and reviews (e.g., Domeisen et al., 2023; Horton et al., 2016; Kalashnikov et al., 2025; Matthews et al., 2025). However, we show that even in an individual location, high thresholds of extreme humid heat in this region can be achieved through modulations of either T_a or humidity. The predominant component of these bivariate drivers toward extreme humid heat has been investigated for individual hotspot regions (C. Ivanovich et al., 2022; Raymond et al., 2017, 2021; Wang et al., 2019) and the statistical variability of drivers has been quantified globally (C. C. Ivanovich, Sobel, et al., 2024). Specific to our study region, Raymond and coauthors (2017) further identified that in the Southwest United States, T_a anomalies drive humid heat extremes in the early part of the heat season while humidity anomalies drive those in the latter half. We extend these findings by linking the T_a and humidity anomalies with regional monsoon dynamics and characterizing the roles of local and advective moisture sources. While we do not explicitly quantify the proportion of humidity stemming from these two sources, both mechanisms are likely at play during WBGT95 events, and we have identified potential contributions within each region. This analysis is also consistent with emerging theories about the interactions of extreme humid heat and precipitation, for example, that extreme humid heat in arid regions tends to be timed closely with enhanced precipitation (Johnson et al., 2024; Speizer et al., 2022). Further, the temporal evolution of meteorological conditions in the week before WBGT95 events in the EDGE region provides an example of high thresholds of extreme humid heat occurring during intermittent precipitation (Jackson et al., 2024; Zhang et al., 2024). The regional exploration provided by the present analysis thus not only characterizes the unique local drivers of extreme humid heat in a major hotspot but also helps to build evidence towards emerging theories about the global drivers of extreme humid heat.

10.1029/2025JD045713

5. Conclusions

These results are significant not only in their scientific novelty but also in their relevance for heat stress resiliency and management. Understanding the risk for both extreme dry and humid heat—and their distinct timing—is especially important for hazard management as the methods for combatting dry and humid heat are not interchangeable. Swamp coolers are a prominent method of extreme dry heat mediation in the Southwest United States (Alger et al., 2020), reducing dry bulb temperatures through evaporating cooling. Although this method is often cheaper than air conditioning using traditional HVAC systems due to lower energy requirements, it can only reduce temperatures based on the deficit between the dry and wet bulb temperatures of the outdoor air, limiting cooling capacity when atmospheric humidity is high (Amer et al., 2015). During humid heat waves, air conditioning is the only effective cooling mechanism (Matthews et al., 2025). Identifying that both types of heat can reach extreme thresholds in this region and characterizing their distinct timing is essential for implementing the correct cooling strategies. Additionally, humid heat of a given threshold, which is primarily composed of high temperatures (rather than high humidity), tends to be more dangerous for human health (Vecellio et al., 2022a, Vecellio et al., 2022b). The results presented here identifying when extremes are driven by T_a versus moisture fluctuations can help discern the most physically threatening extreme event types.

We also devise a new method for identifying the start, peak, and end of extreme heat seasons, which can be applied widely to compare spatial and temporal variations in heat seasonality, using any heat stress metric of choice. Here we quantify average heat season characteristics over the historical period, but this definition also provides consistent metrics to evaluate heat season variability and trends which have previously been underexplored (Ha et al., 2022; Son et al., 2022; Wang et al., 2021). For example, these metrics could be used to investigate the interactions between the evolving North American Monsoon season and local heat seasons with ongoing climate change. Research has shown that different types of extreme heat can occur when the South Asian Summer Monsoon onset is early or delayed (C. C. Ivanovich, Horton, et al., 2024) and has suggested that increasing trends for regional extreme heat frequency in Southeastern Brazil may be linked to a shortening of the South American Monsoon active season (C. C. Ivanovich et al., 2025). With future anthropogenic climate change, the North American Monsoon is projected to experience delayed onset and withdrawal, though there is disagreement over how the total monsoon precipitation will change (Cook & Seager, 2013; Hoell et al., 2016; Pascale et al., 2017). Future work should explore how the seasonality of monsoon precipitation interacts with the frequency and timing of extreme heat historically and in the future as the North American Monsoon season continues to evolve.

The widespread negative soil moisture anomalies during months with a high frequency of WBGT95 events in CORE further raise the seemingly counterintuitive question of whether humid heat events can take place during large-scale droughts. A significant body of literature has been devoted to exploring the historic and future intersection of compound extreme dry heat and drought events (e.g., Geirinhas et al., 2021; Mukherjee & Mishra, 2021; C. Wang et al., 2024), as the dynamics of surface drying and extreme T_a are often intertwined and nonlinear. However, during a drought defined by lack of precipitation and declines in soil moisture, a brief injection of surface moisture from light, intermittent precipitation, or advection of humid air from surrounding water bodies or moist land could trigger short-term extreme humid heat events without ending drought conditions. Similar mechanisms have been highlighted as triggering high intensity humid heat extremes in climatologically arid and semi-arid regions (Duan et al., 2025; Zhang et al., 2024). Indeed, the Southwest United States has been in a long-term drought for decades (Williams et al., 2022), and any WBGT95 events during this period could be considered compound drought-humid heat events. Compound climate extremes have outsized impacts relative to the sum of their individual parts (Zscheischler et al., 2018, 2020), and drought and extreme humid heat can both impact agricultural production through their influence over plant and human health (Diaz et al., 2023; Schauberger et al., 2017; Ting et al., 2023). Improving our understanding of the potential intersection of extreme humid heat and drought is therefore essential for monitoring, management, and adaptation planning.

Conflict of Interest

The authors declare no conflicts of interest relevant to this study.

Availability Statement

The publicly available datasets used in this analysis are accessible via the following websites: MERRA2 (Gelaro et al., 2017), https://gmao.gsfc.nasa.gov/reanalysis/merra-2/data_access/; and ERA5 (Hersbach et al., 2020), https://cds.climate.copernicus.eu/datasets/reanalysis-era5-single-levels?tab=overview and https://cds.climate.copernicus.eu/datasets/reanalysis-era5-pressure-levels?tab=overview. All code for analysis and figure production is publicly available on GitHub at https://github.com/ccivanovich/NAM_Extreme_Heat and is preserved on Zenodo at https://doi.org/10.5281/zenodo.17353220. Figures were made with Matplotlib (Hunter, 2007) and Cartopy (Met Office, 2015), available at https://matplotlib.org/stable/ and https://scitools.org.uk/cartopy/docs/v0.15/citation.html, respectively. Analysis was completed using Xarray (Hoyer & Hamman, 2017) and SciPy (Virtanen et al., 2020), available at https://docs.xarray.dev/en/latest/index.html and https://scipy.org/, respectively.

Acknowledgments

C. I. is supported by the NASA Postdoctoral Program (NPP) Fellowship (ORAU-80HQTR21CA005). Research was sponsored by the National Aeronautics and Space Administration (NASA) through a contract with ORAU. The views and conclusions contained in this document are those of the authors and should not be interpreted as representing the official policies, either expressed or implied, of the National Aeronautics and Space Administration (NASA) or the U.S. Government. The U.S. The Government is authorized to reproduce and distribute reprints for Government purposes notwithstanding any copyright notation herein. B. C. supported by the NASA Modeling, Analysis, and Prediction program.

References

Abatzoglou, J. T., & Williams, A. P. (2016). Impact of anthropogenic climate change on wildfire across Western US forests. *Proceedings of the National Academy of Sciences*, *113*(42), 11770–11775. https://doi.org/10.1073/pnas.1607171113

Adams, D. K., & Comrie, A. C. (1997). The north American monsoon. *Bulletin of the American Meteorological Society*, *78*(10), 2197–2213. https://doi.org/10.1175/1520-0477(1997)078<253C2197:TNAM>253E2.0.CO;2

Alger, J., Mayer, A., Kumar, S., & Granados-Olivas, A. (2020). Urban evaporative consumptive use for water-scarce cities in the United States and Mexico. *AWWA Water Science*, *2*(5), e1185. https://doi.org/10.1002/aws2.1185

Ambika, A. K., Rajeev, A., & Huber, M. (2024). Global warming amplifies outdoor extreme moist heat during the Indian summer monsoon. *Earth's Future*, *12*(7), e2024EF004673. https://doi.org/10.1029/2024EF004673

Amer, O., Boukhanouf, R., Nottingham, U. K., & Ibrahim, H. G., & The University of Nottingham, Department of Built Environment, Qatar University, the Department of Architecture and Urban Planning, Doha, Qatar. (2015). A review of evaporative cooling technologies. *International Journal of Environment and Sustainable Development*, *6*(2), 111–117. https://doi.org/10.7763/IJESD.2015.V6.571

Asseng, S., Spänkuch, D., Hernandez-Ochoa, I. M., & Laporta, J. (2021). The upper temperature thresholds of life. *The Lancet Planetary Health*, *5*(6), e378–e385. https://doi.org/10.1016/S2542-5196(21)00079-6

Bekris, Y., Loikith, P. C., & Neelin, J. D. (2023). Short warm distribution tails accelerate the increase of humid-heat extremes under global warming. *Geophysical Research Letters*, *50*(11), e2022GL102164. https://doi.org/10.1029/2022GL102164

Binkley, H. M., Beckett, J., Casa, D. J., Kleiner, D. M., & Plummer, P. E. (2002). National athletic trainers' Association position statement: Exertional heat illnesses. *Journal of Athletic Training*, *37*(3), 329–343.

Boos, W. R., & Pascale, S. (2021). Mechanical forcing of the North American monsoon by orography. *Nature*, *599*(7886), 611–615. https://doi.org/10.1038/s41586-021-03978-2

Bowman, D. M. J. S., Balch, J. K., Artaxo, P., Bond, W. J., Carlson, J. M., Cochrane, M. A., et al. (2009). Fire in the Earth system. *Science*, *324*(5926), 481–484. https://doi.org/10.1126/science.1163886

Brimicombe, C., Di Napoli, C., Quintino, T., Pappenberger, F., Cornforth, R., & Cloke, H. L. (2022). Thermofeel: A python thermal comfort indices library. *SoftwareX*, *18*, 101005. https://doi.org/10.1016/j.softx.2022.101005

Budd, G. M. (2008). Wet-bulb globe temperature (WBGT)—Its history and its limitations. *Journal of Science and Medicine in Sport*, *11*(1), 20–32. https://doi.org/10.1016/j.jsams.2007.07.003

Buzan, J. R., Oleson, K., & Huber, M. (2015). Implementation and comparison of a suite of heat stress metrics within the Community Land Model version 4.5. *Geoscientific Model Development*, *8*(2), 151–170. https://doi.org/10.5194/gmd-8-151-2015

Buzan, J. R., & Huber, M. (2020). Moist heat stress on a hotter Earth. *Annual Review of Earth and Planetary Sciences*, *48*(1), 623–655. https://doi.org/10.1146/annurev-earth-053018-060100

Chow, D. (2024). Phoenix ends 21-day streak of record October heat. NBC News. Retrieved from https://www.nbcnews.com/science/climate-change/phoenix-fall-heat-wave-records-october-rcna175349

Cook, B. I., & Buckley, B. M. (2009). Objective determination of monsoon season onset, withdrawal, and length. *Journal of Geophysical Research*, *114*(D23), 2009JD012795. https://doi.org/10.1029/2009JD012795

Cook, B. I., & Seager, R. (2013). The response of the North American Monsoon to increased greenhouse gas forcing. *Journal of Geophysical Research: Atmospheres*, *118*(4), 1690–1699. https://doi.org/10.1002/jgrd.50111

Cueto, R. O. G., Martínez, A. T., & Ostos, E. J. (2010). Heat waves and heat days in an arid city in the northwest of México: Current trends and in climate change scenarios. *International Journal of Biometeorology*, *54*(4), 335–345. https://doi.org/10.1007/s00484-009-0283-7

De Dear, R. (1987). Ping-pong globe thermometers for mean radiant temperatures. *H and V Engineer*, *60*(681), 10–11.

De Freitas, C., & Grigorieva, E. (2015). Role of acclimatization in weather-related human mortality during the transition seasons of autumn and Spring in a thermally extreme mid-latitude Continental climate. *International Journal of Environmental Research and Public Health*, *12*(12), 14974–14987. https://doi.org/10.3390/ijerph121214962

Diaz, C. D., Ting, M., Horton, R. M., Singh, D., Rogers, C. D. W., & Coffel, E. D. (2023). Increased extreme humid heat hazard faced by agricultural workers. *Environmental Research Communications*, *5*(11), 115013. https://doi.org/10.1088/2515-7620/ad028d

Di Napoli, C., Hogan, R. J., & Pappenberger, F. (2020). Mean radiant temperature from global-scale Numerical weather prediction models. *International Journal of Biometeorology*, *64*(7), 1233–1245. https://doi.org/10.1007/s00484-020-01900-5

Domeisen, D. I. V., Eltahir, E. A. B., Fischer, E. M., Knutti, R., Perkins-Kirkpatrick, S. E., Schär, C., et al. (2023). Prediction and projection of heatwaves. *Nature Reviews Earth and Environment*, *4*(1), 36–50. https://doi.org/10.1038/s43017-022-00371-z

Dong, J., Brönnimann, S., Hu, T., Cheng, X., Liu, Y., & Peng, J. (2024). Trends of the intra-annual onset and end of humid heatwaves in the Northern hemisphere. *Earth's Future*, *12*(11), e2024EF005163. https://doi.org/10.1029/2024EF005163

Duan, S. Q., McKinnon, K. A., & Simpson, I. R. (2025). The impact of soil preconditioning on the evolution of heatwaves under constrained circulation: A case Study of the 2021 Pacific Northwest heatwave. *Earth's Future*, *13*(9), e2025EF006216. https://doi.org/10.1029/2025EF006216

Engdaw, M. M., Ballinger, A. P., Hegerl, G. C., & Steiner, A. K. (2022). Changes in temperature and heat waves over Africa using observational and reanalysis data sets. *International Journal of Climatology*, *42*(2), 1165–1180. https://doi.org/10.1002/joc.7295

Fanger, P. O. (1970). *Thermal comfort: Analysis and applications in environmental engineering*. Danish Technical Press.

Freedman, A. (2024). Phoenix shatters extreme heat records into fall. *Axios*. Retrieved from https://www.axios.com/2024/10/17/phoenix-shatters-heat-records-fall

Geirinhas, J. L., Russo, A., Libonati, R., Sousa, P. M., Miralles, D. G., & Trigo, R. M. (2021). Recent increasing frequency of compound summer drought and heatwaves in Southeast Brazil. *Environmental Research Letters*, *16*(3), 034036. https://doi.org/10.1088/1748-9326/abe0eb

Gelaro, R., McCarty, W., Suárez, M. J., Todling, R., Molod, A., Takacs, L., et al. (2017). The modern-era retrospective analysis for research and applications, version 2 (MERRA-2) [Dataset]. *Journal of Climate*, *30*(14), 5419–5454. https://doi.org/10.1175/JCLI-D-16-0758.1

Grundstein, A., & Vanos, J. (2021). There is no "Swiss Army Knife" of thermal indices: The importance of considering "why?" and "for whom?" when modelling heat stress in sport. *British Journal of Sports Medicine*, *55*(15), 822–824. https://doi.org/10.1136/bjsports-2020-102920

Grundstein, A., Williams, C., Phan, M., & Cooper, E. (2015). Regional heat safety thresholds for athletics in the contiguous United States. *Applied Geography*, *56*, 55–60. https://doi.org/10.1016/j.apgeog.2014.10.014

Guirguis, K., Gershunov, A., Cayan, D. R., & Pierce, D. W. (2018). Heat wave probability in the changing climate of the Southwest US. *Climate Dynamics*, *50*(9–10), 3853–3864. https://doi.org/10.1007/s00382-017-3850-3

Ha, K.-J., Seo, Y.-W., Yeo, J.-H., Timmermann, A., Chung, E.-S., Franzke, C. L. E., et al. (2022). Dynamics and characteristics of dry and moist heatwaves over East Asia. *npj Climate and Atmospheric Science*, *5*(1), 49. https://doi.org/10.1038/s41612-022-00272-4

Hersbach, H., Bell, B., Berrisford, P., Hirahara, S., Horányi, A., Muñoz-Sabater, J., et al. (2020). The ERA5 global reanalysis [Dataset]. *Quarterly Journal of the Royal Meteorological Society*, *146*(730), 1999–2049. https://doi.org/10.1002/qj.3803

Hirschi, M., Stradiotti, P., Crezee, B., Dorigo, W., & Seneviratne, S. I. (2025). Potential of long-term satellite observations and reanalysis products for characterising soil drying: Trends and drought events. *Hydrology and Earth System Sciences*, *29*(2), 397–425. https://doi.org/10.5194/hess-29-397-2025

Hoell, A., Funk, C., Barlow, M., & Shukla, S. (2016). Recent and possible future variations in the north American monsoon. In L. M. V. De Carvalho & C. Jones (Eds.), *The monsoons and climate change* (pp. 149–162). Springer International Publishing. https://doi.org/10.1007/978-3-319-21650-8_7

Horton, R. M., Mankin, J. S., Lesk, C., Coffel, E., & Raymond, C. (2016). A review of recent advances in research on extreme heat events. *Current Climate Change Reports*, *2*(4), 242–259. https://doi.org/10.1007/s40641-016-0042-x

Hoyer, S., & Hamman, J. (2017). Xarray: N-D labeled Arrays and Datasets in Python [Software]. *Journal of Open Research Software*, *5*(1), 10. https://doi.org/10.5334/jors.148

Hunter, J. D. (2007). Matplotlib: A 2D graphics environment [Software]. *Computing in Science and Engineering*, *9*(3), 90–95. https://doi.org/10.1109/MCSE.2007.55

Ivanovich, C., Anderson, W., Horton, R., Raymond, C., & Sobel, A. (2022). The influence of intraseasonal oscillations on humid heat in the Persian Gulf and south Asia. *Journal of Climate*, *35*(13), 4309–4329. https://doi.org/10.1175/JCLI-D-21-0488.1

Ivanovich, C. C., Horton, R. M., Sobel, A. H., & Singh, D. (2024). Subseasonal variability of humid heat during the South Asian summer monsoon. *Geophysical Research Letters*, *51*(6), e2023GL107382. https://doi.org/10.1029/2023GL107382

Ivanovich, C. C., Sobel, A. H., Horton, R. M., Nunes, A. M. B., Da Rocha, R. P., & Camargo, S. J. (2025). Physical drivers of the November 2023 heatwave in Rio de Janeiro. *Weather and Climate Dynamics*, *6*(4), 1857–1874. https://doi.org/10.5194/wcd-6-1857-2025

Ivanovich, C. C., Sobel, A. H., Horton, R. M., & Raymond, C. (2024). Stickiness: A new variable to characterize the temperature and humidity contributions toward humid heat. *Journal of the Atmospheric Sciences*, *81*(5), 819–837. https://doi.org/10.1175/JAS-D-23-0072.1

Jackson, L., Birch, C., Chagnaud, G., Marsham, J., & Taylor, C. (2024). Humid heatwaves are controlled by daily rainfall variability. https://doi.org/10.21203/rs.3.rs-5037159/v1

Johnson, S., Ivanovich, C., Horton, R. M., Ting, M., Kornhuber, K., & Lesk, C. (2024). Temporal connections between extreme precipitation and humid heat. *Environmental Research Letters*, *19*(11), 114076. https://doi.org/10.1088/1748-9326/ad7edc

Kalashnikov, D. A., Singh, D., Ting, M., & Cook, B. I. (2025). Contributions of atmospheric ridging and low soil moisture to the record-breaking June 2023 mexico-texas heatwave. *Geophysical Research Letters*, *52*(5), e2025GL114987. https://doi.org/10.1029/2025GL114987

Khan, N., Ahmad, S., & Shahid, S. (2025). Assessing the deadly heat waves over South Asian cities: An insights from UTCI and WBGT indices. *International Journal of Climatology*, *45*(7), e8806. https://doi.org/10.1002/joc.8806

Kimmel, T. M., Nielsen-Gammon, J., Rose, B., & Mogil, H. M. (2016). The weather and climate of Texas: A big State with big extremes. *Weatherwise*, *69*(5), 25–33. https://doi.org/10.1080/00431672.2016.1206446

Liljegren, J. C., Carhart, R. A., Lawday, P., Tschopp, S., & Sharp, R. (2008). Modeling the wet Bulb globe temperature using standard meteorological measurements. *Journal of Occupational and Environmental Hygiene*, *5*(10), 645–655. https://doi.org/10.1080/15459620802310770

Lizárraga-Celaya, C., Watts, C. J., Rodríguez, J. C., Garatuza-Payán, J., Scott, R. L., & Sáiz-Hernández, J. (2010). Spatio-temporal variations in surface characteristics over the North American Monsoon region. *Journal of Arid Environments*, *74*(5), 540–548. https://doi.org/10.1016/j.jaridenv.2009.09.027

Matthews, T., Raymond, C., Foster, J., Baldwin, J. W., Ivanovich, C., Kong, Q., et al. (2025). Mortality impacts of the most extreme heat events. *Nature Reviews Earth and Environment*, *6*(3), 193–210. https://doi.org/10.1038/s43017-024-00635-w

McKinnon, K. A., Poppick, A., & Simpson, I. R. (2021). Hot extremes have become drier in the United States Southwest. *Nature Climate Change*, *11*(7), 598–604. https://doi.org/10.1038/s41558-021-01076-9

Met Office. (2015). Cartopy: A cartographic python library with a matplotlib interface [Software]. *Exeter, Devon*. Retrieved from http://scitools.org.uk/cartopy

Mitchell, D. L., Ivanova, D., Rabin, R., Brown, T. J., & Redmond, K. (2002). Gulf of California Sea surface temperatures and the north American monsoon: Mechanistic implications from observations. *Journal of Climate*, *15*(17), 2261–2281. https://doi.org/10.1175/1520-0442(2002)015<2261:GOCSST>2.0.CO;2

Mora, C., Dousset, B., Caldwell, I. R., Powell, F. E., Geronimo, R. C., Bielecki, C. R., et al. (2017). Global risk of deadly heat. *Nature Climate Change*, *7*(7), 501–506. https://doi.org/10.1038/nclimate3322

Mukherjee, S., & Mishra, A. K. (2021). Increase in compound drought and heatwaves in a warming world. *Geophysical Research Letters*, *48*(1), e2020GL090617. https://doi.org/10.1029/2020GL090617

Mutiibwa, D., Vavrus, S. J., McAfee, S. A., & Albright, T. P. (2015). Recent spatiotemporal patterns in temperature extremes across conterminous United States. *Journal of Geophysical Research: Atmospheres*, *120*(15), 7378–7392. https://doi.org/10.1002/2015JD023598

Navarro-Estupiñan, J., Robles-Morua, A., Vivoni, E. R., Zepeda, J. E., Montoya, J. A., & Verduzco, V. S. (2018). Observed trends and future projections of extreme heat events in Sonora, Mexico. *International Journal of Climatology*, *38*(14), 5168–5181. https://doi.org/10.1002/joc.5719

OSHA Technical Manual. (2017). U.S. Department of Labor, occupational safety and health administration. Retrieved from https://www.osha.gov/otm/

Parajuli, S. P., Biggs, T., Galvez, N. L., Quintana, P., Ciborowski, H., De Sales, F., et al. (2025). Heat-related rest-break recommendations for farmworkers in California based on wet-bulb globe temperature. *Communications Earth and Environment*, *6*(1), 1–13. https://doi.org/10.1038/s43247-025-02327-9

Parsons, K. (2006). Heat stress standard ISO 7243 and its global application. *Industrial Health*, *44*(3), 368–379. https://doi.org/10.2486/indhealth.44.368

Pascale, S., Boos, W. R., Bordoni, S., Delworth, T. L., Kapnick, S. B., Murakami, H., et al. (2017). Weakening of the North American monsoon with global warming. *Nature Climate Change*, *7*(11), 806–812. https://doi.org/10.1038/nclimate3412

Perkins-Kirkpatrick, S. E., & Lewis, S. C. (2020). Increasing trends in regional heatwaves. *Nature Communications*, *11*(1), 3357. https://doi.org/10.1038/s41467-020-16970-7

Raymond, C., Matthews, T., & Horton, R. M. (2020). The emergence of heat and humidity too severe for human tolerance. *Science Advances*, *6*(19), eaaw1838. https://doi.org/10.1126/sciadv.aaw1838

Raymond, C., Matthews, T., Horton, R. M., Fischer, E. M., Fueglistaler, S., Ivanovich, C., et al. (2021). On the controlling factors for globally extreme humid heat. *Geophysical Research Letters*, *48*(23), e2021GL096082. https://doi.org/10.1029/2021GL096082

Raymond, C., Shreevastava, A., Slinskey, E., & Waliser, D. (2024). Linkages between atmospheric rivers and humid heat across the United States. *Natural Hazards and Earth System Sciences*, *24*(3), 791–801. https://doi.org/10.5194/nhess-24-791-2024

Raymond, C., Singh, D., & Horton, R. M. (2017). Spatiotemporal patterns and synoptics of extreme wet-bulb temperature in the contiguous United States: U.S. Extreme-WBT patterns. *Journal of Geophysical Research: Atmospheres*, *122*(24), 13108–13124. https://doi.org/10.1002/2017JD027140

Rogers, C. D. W., Ting, M., Li, C., Kornhuber, K., Coffel, E. D., Horton, R. M., et al. (2021). Recent increases in exposure to extreme humid-heat events disproportionately affect populated regions. *Geophysical Research Letters*, *48*(19), e2021GL094183. https://doi.org/10.1029/2021GL094183

Schauberger, B., Archontoulis, S., Arneth, A., Balkovic, J., Ciais, P., Deryng, D., et al. (2017). Consistent negative response of US crops to high temperatures in observations and crop models. *Nature Communications*, *8*(1), 13931. https://doi.org/10.1038/ncomms13931

Sheppard, P., Comrie, A., Packin, G., Angersbach, K., & Hughes, M. (2002). The climate of the US Southwest. *Climate Research*, *21*, 219–238. https://doi.org/10.3354/cr021219

Sherwood, S. C., & Huber, M. (2010). An adaptability limit to climate change due to heat stress. *Proceedings of the National Academy of Sciences*, *107*(21), 9552–9555. https://doi.org/10.1073/pnas.0913352107

Shonk, J. K. P., Blunn, L. P., Kumar, V., Wurtz, J., & Masson, V. (2026). UCanWBGT: Urban street canyon heat stress calculation for weather and climate models. *Quarterly Journal of the Royal Meteorological Society*, *152*(776), e70082. https://doi.org/10.1002/qj.70082

Son, J.-H., Kim, N.-H., Kim, G.-U., Chu, J.-E., Park, J.-H., Kwon, J., & Heo, K.-Y. (2022). Early-onset trend in European summer caused by Greenland topographic effect. *Environmental Research Letters*, *17*(10), 104039. https://doi.org/10.1088/1748-9326/ac94e7

Speizer, S., Raymond, C., Ivanovich, C., & Horton, R. M. (2022). Concentrated and intensifying humid heat extremes in the IPCC AR6 regions. *Geophysical Research Letters*, *49*(5), e2021GL097261. https://doi.org/10.1029/2021GL097261

Steadman, R. G. (1979). The assessment of sultriness. Part I: A temperature-humidity index based on human physiology and clothing science. *Journal of Applied Meteorology and Climatology*, *18*(7), 861–873. https://doi.org/10.1175/1520-0450(1979)018<0861:TAOSPI>2.0.CO;2

Ting, M., Lesk, C., Liu, C., Li, C., Horton, R. M., Coffel, E. D., et al. (2023). Contrasting impacts of dry versus humid heat on US corn and soybean yields. *Scientific Reports*, *13*(1), 710. https://doi.org/10.1038/s41598-023-27931-7

Vanos, J. K., & Grundstein, A. J. (2020). Variations in athlete heat-loss potential between hot-dry and warm-humid environments at equivalent wet-bulb globe temperature thresholds. *Journal of Athletic Training*, *55*(11), 1190–1198. https://doi.org/10.4085/1062-6050-313-19

Vecellio, D. J., Wolf, S. T., Cottle, R. M., & Kenney, W. L. (2022a). Evaluating the 35°C wet-bulb temperature adaptability threshold for young, healthy subjects (PSU HEAT Project). *Journal of Applied Physiology*, *132*(2), 340–345. https://doi.org/10.1152/japplphysiol.00738.2021

Vecellio, D. J., Wolf, S. T., Cottle, R. M., & Kenney, W. L. (2022b). Utility of the Heat Index in defining the upper limits of thermal balance during light physical activity (PSU HEAT Project). *International Journal of Biometeorology*, *66*(9), 1759–1769. https://doi.org/10.1007/s00484-022-02316-z

Virtanen, P., Gommers, R., Oliphant, T. E., Haberland, M., Reddy, T., Cournapeau, D., et al. (2020). SciPy 1.0: Fundamental algorithms for scientific computing in Python [Software]. *Nature Methods*, *17*(3), 261–272. https://doi.org/10.1038/s41592-019-0686-2

Wang, C., Li, Z., Chen, Y., Ouyang, L., Zhao, H., Zhu, J., et al. (2024). Characteristic changes in compound drought and heatwave events under climate change. *Atmospheric Research*, *305*, 107440. https://doi.org/10.1016/j.atmosres.2024.107440

Wang, J., Guan, Y., Wu, L., Guan, X., Cai, W., Huang, J., et al. (2021). Changing lengths of the four seasons by global warming. *Geophysical Research Letters*, *48*(6), e2020GL091753. https://doi.org/10.1029/2020GL091753

Wang, P., Leung, L. R., Lu, J., Song, F., & Tang, J. (2019). Extreme wet-bulb temperatures in China: The significant role of moisture. *Journal of Geophysical Research: Atmospheres*, *124*(22), 11944–11960. https://doi.org/10.1029/2019JD031477

Williams, A. P., Cook, B. I., & Smerdon, J. E. (2022). Rapid intensification of the emerging southwestern North American megadrought in 2020–2021. *Nature Climate Change*, *12*(3), 232–234. https://doi.org/10.1038/s41558-022-01290-z

Zhang, Z., Wang, Y., Zhang, G. J., Xing, C., Xia, W., & Yang, M. (2024). Light rain exacerbates extreme humid heat. *Nature Communications*, *15*(1), 7326. https://doi.org/10.1038/s41467-024-51778-9

Zscheischler, J., Martius, O., Westra, S., Bevacqua, E., Raymond, C., Horton, R. M., et al. (2020). A typology of compound weather and climate events. *Nature Reviews Earth and Environment*, *1*(7), 333–347. https://doi.org/10.1038/s43017-020-0060-z

Zscheischler, J., Westra, S., van den Hurk, B. J. J. M., Seneviratne, S. I., Ward, P. J., Pitman, A., et al. (2018). Future climate risk from compound events. *Nature Climate Change*, *8*(6), 469–477. https://doi.org/10.1038/s41558-018-0156-3